Generation of 20-GHz picosecond pulse trains in the normal and anomalous dispersion regimes of optical fibers

Stéphane Pitois, Christophe Finot, Julien Fatome, Bernard Sinardet, Guy Millot

Generation of 20-GHz picosecond pulse trains in the normal and anomalous dispersion regimes of optical fibers

Stéphane Pitois, Christophe Finot, Julien Fatome,
Bernard Sinardet and Guy Millot

Laboratoire de Physique de l'Université de Bourgogne, Unité Mixte de Recherche 5027, Centre National de la Recherche Scientifique, Faculté des Sciences Mirande, 9 Avenue Alain Savary, B.P. 47870, 21078 Dijon Cédex, France

Abstract

In this paper, we numerically and experimentally study two methods to generate 20-GHz pulse trains at 1550 nm from a dual-frequency beat-signal. The first method is based on the multiple four-wave mixing temporal compression occuring in the anomalous dispersion regime of a standard optical fiber (SMF). In the second original method, the initial sinusoidal signal is first converted into a parabolic pulses train through nonlinear propagation in a normally dispersive fiber. A subsequent linear compression in an anomalous dispersive fiber leads to well-separated picosecond pulses.

1 Introduction

Nonlinear transformation of a dual-frequency beat-signal into a well-separated pulses train is a powerful method to generate picosecond pulses at very high repetition rates ($\geq$ 40 GHz). These nonlinear beat-conversion techniques are mainly based on modulational instability ; , soliton-assisted compression ; or switching in a nonlinear optical loop mirror (NOLM) . Recently, a simple method using multiple four-wave mixing in the anomalous-dispersion regime of a nonzero dispersion-shifted fiber has been investigated to generate high-quality picosecond pulses at 160 GHz . However, only train of "ones" can be generated and presently available optical modulators are not able to code data at bit rates higher than 40 Gbit/s. Therefore, an alternative approach, namely the OTDM (Optical Time Division Multiplexing), consists of generating picosecond pulses at moderate repetition rate (10 Gbit/s or 20 Gbit/s) with a high mark-space ratio, coding them and finally using a temporal multiplexer

to obtain coded pulse trains at 40 Gbit/s or more. In this paper, we present and compare numerically and experimentally two simple methods to generate such picosecond pulse trains at 20 GHz. The paper is organized as follow : in a first part, we present a method based on multiple four-wave mixing occuring in the anomalous dispersion regime of a SMF fiber. Numerical and experimental results show that high quality pulse trains are generated. In the second part, we focus our attention on another method which is based on the generation of parabolic pulses in the normal dispersion regime of a non-zero dispersion-shifted fiber (NZ-DSF). After linear compression of these parabolic pulses by chirp compensation in a SMF, well-separated picosecond pulses are generated. Frequency resolved optical gating (FROG) measurements were also used to give access to both intensity and phase profiles of the compressed pulses . Finally, the last section draws a comparison between the two methods.

2 Compression through multiple four-wave mixing

This first method is based on the temporal compression of a dual-frequency beat-signal in the anomalous dispersion regime of a standard optical fiber (SMF) . The initial sinusoidal signal can be obtained from the beating of two cw laser diodes or directly by the external modulation of a single cw laser. Due to the combined effects of nonlinearity (Kerr effect) and anomalous dispersion, the two initial frequencies at ω_1 and ω_2 interact and create new waves at frequencies $\omega_1 - \Omega$ and $\omega_2 + \Omega$, where $\Omega = \omega_2 - \omega_1$. Then, due to multiple four-wave mixing processes, many harmonic bands are generated, leading to a strong spectral broadening. This spectral broadening is then accompagnied by a strong temporal compression of the sinusoidal signal in a picosecond well-separated pulse train .

2.1 Description of the experimental set-up

Figure 1a represents the experimental set-up used to generate the 20-GHz pulse train. The initial beat signal was obtained from two cw 150-kHz-linewidth tunable-wavelength external-cavity laser diodes frequency separated by 20 GHz. Both waves were combined by a 50:50 coupler and then amplified to the desired average power by means of a polarization-maintening (PM) Erbium-doped fiber amplifier (EDFA). A LiNbO3 phase modulator, driven at a frequency of 130 MHz, was also used to increase the stimulated Brillouin scattering threshold well above the power used in our experiment. The central wavelength of the laser diodes was fixed to 1550 nm. The beat signal is then injected into a SMF fiber with the following parameters : length $L = 7900$ m, linear losses $\alpha = 0.3$ dB/km, group-velocity dipsersion $D = 17$ ps/nm/km,

slope $S = 0.055$ ps/nm^2/km, effective area $A_{eff} = 80\ \mu$m^2 and nonlinear coefficient $\gamma = 1.3$ W^{-1} km^{-1}. The output field was characterized with an optical spectrum analyser (OSA), a background-free second-harmonic-generation autocorrelator and a FROG setup based on the spectral analysis of the second-harmonic-generation autocorrelation signal .

2.2 Theoretical model and numerical simulations

Propagation of the beat signal in a SMF fiber is ruled by the following nonlinear Schrödinger equation :

$$\frac{\partial A}{\partial z} + \frac{i}{2}\beta_2 \frac{\partial^2 A}{\partial t^2} - \frac{1}{6}\beta_3 \frac{\partial^3 A}{\partial t^3} + \frac{\alpha}{2} A = i\gamma \mid A \mid^2 A \ , \tag{1}$$

where $A(z,t)$ is the slowly varying amplitude of the electric field. β_2 and β_3 are the second- and third- dispersion coefficients, respectively. γ is the usual nonlinear coefficient, and α represents the fiber losses. Eq.(1) was integrated numerically by means of a standard split-step Fourier method with the fiber parameters given in the description of the experimental set-up. The optimum input average power, for a maximum compression and mimimum chirp was found to $P_0 = 120$ mW. Figure 2 illustrates the temporal compression of the dual-frequency pump field obtained for $\lambda = 1550$ nm. Dashed line in Fig. 2a represents the intensity profile of the sinusoidal input field at z = 0. The corresponding spectrum, which illustrates the two initial frequencies spaced by 20 GHz, is also represented in Fig. 2c . The generated pulse train at z = 7900 m is represented in Fig. 2a (solid line) whereas Fig. 2b shows the corresponding nearly flat phase profile. The spectral broadening induced by multiple FWM is clearly visible in Fig. 2d. The output pulses have a nearly Gaussian intensity profile with a 11 ps FWHM.

2.3 Experimental results

The experimental results obtained at $\lambda = 1550$ nm are shown in Fig. 3. Maximum compression was obtained for an input average power of $P_0 = 130$ mW, in good agreement with the theoretical value. The FROG technique, adapted for high-repetition-rate periodic pulse trains was used to characterize directly the intensity and phase of the 20-GHz pulse train . The measured and retrieved FROG traces (128 $\times$ 128 grid) are shown in Fig. 3c and Fig. 3d, respectively. The retrieval error, defined as the rms between the original and retrieved FROG traces, was found to be $\epsilon = 8.10^{-3}$. The retrieved intensity

profile is shown in Fig. 3a (solid line), as well as our numerical predictions (circles). We can clearly observe an excellent agreement between experimental results and numerical simulations, confirming the reability of this technique. The retrieved phase profile is also shown in Fig. 1b and is found to be quite flat over the entire pulse width, indicating that pulses are nearly transform-limited. Moreover, as preticted from numerical simulations, a π phase shift is observed between consecutive pulses. Note that the SHG-FROG technique has an unavoidable ambiguity in the direction of time due to its second-order process nature. Therefore the time direction was determined by drawing a direct comparison between the retrieved pulses and numerical simulations.

Finally, for a constant input average power of $P_0 = 130$ mW, we have checked the tunability of our source by studying the variation of the output pulse shapes as a function of the central wavelength. Autocorrelation traces and corresponding spectra, represented in Fig. 4 for three different central wavelength between 1545 nm and 1565 nm, are found to be very similar. Indeed, the wavelength tunability of the compression technique is essentially limited by the ASE (amplified-spontaneous emission) bandwidth of our EDFA (erbium-doped fiber amplifier).

3 Compression by parabolic pulse train generation

The second original method of 20 GHz pulse train generation we have performed is based on the transformation of the initial sinusoidal beat-signal into a train of linearly-chirped quasi-parabolic pulses. This transformation occurs due to the combined effects of self-phase modulation and normal dispersion in a non zero dispersion shifted fiber. After linear compression of the parabolic pulses into an optical fiber with opposite dispersion (1.8 km of SMF), a train of 5.5 ps well-separated pulses is obtained.

3.1 Description of the experimental set-up

Figure 1b represents the experimental set-up used to generate the 20-GHz pulse train. First, the sinusoidal signal is injected into a NZ-DSF fiber with the following parameters : length $L_1 = 5300$ m, linear losses $\alpha_1 = 0.22$ dB/km, group-velocity dispersion D_1 = -3.2 ps/nm/km, slope $S_1 = 0.06$ ps/nm^2/km and effective area $A_{eff1} = 50$ μm^2 and nonlinear coefficient $\gamma_1 = 2.2$ W^{-1} km^{-1}. A 10 dB attenuator was located after the NZ-DSF to obtain quasi-linear propagation in the compression fiber. The anomalous dispersive compression fiber is a SMF fiber with the following parameters : length $L_2 = 1800$ m, linear losses $\alpha_2 = 0.33$ dB/km, group-velocity dipsersion $D_2 = 17.1$ ps/nm/km,

slope $S_2 = 0.055$ ps/nm^2/km and effective area $A_{eff2} = 80$ μm^2 and nonlinear coefficient $\gamma_2 = 1.3$ W^{-1} km^{-1}. Finally, the output field was characterized by means of the same methods as those used previously. Note that the linear compression stage could also be performed in an anomalous-dispersive air-core photonic bandgap fiber or in fiber gratings ; . Since light propagation in such a fiber is essentially linear, there is no need to attenuate the light power at the fiber input.

3.2 Theoretical model and numerical simulations

Propagation of the beat-signal in NZ-DSF fiber is ruled by Eq. (1). Following Ref. , it may be useful to define the following parameter N :

$$N^2 = \frac{\gamma P_p T_0^2}{\mid \beta_2 \mid} \tag{2}$$

where P_p is the signal peak power and T_0 the initial pulse width. Indeed, N governs the relative role of the SPM and GVD effects on pulse evolution along the fiber length. For N $\gg$ 1, which is the case here (N $\simeq$ 16), and in the normal dispersion regime, it has been shown that an initial isolated Gaussian pulse is transformed into a nearly parabolic pulse accompagnied by a quasi-linear chirp . Consequently, this linear chirp allows to compress efficiently the pulse by passing it though a linear dispersive medium. In fact, numerical simulations show that a sinusoidal signal also evolves towards a parabolic pulse train. This behaviour is illustrated in Fig. 5 where Eq.(1) has been integrated numerically with the fiber parameters given above. Basically, the transformation of sinusoidal pulses into parabolic pulses is due to the combined effects of the weak normal dispersion and the strong SPM-induced frequency chirp. Here, we would like to comment the difference between the parabolic pulses generated in our experiment and those generally generated in normally-dispersive nonlinear amplifiers. Let us recall that pulses injected in a normally-dispersive nonlinear amplifier evolve asymptotically towards linearly chirped parabolic pulses and propagate in the fiber amplifier in an auto-similarly way (i.e. after a certain propagation distance, the pulses have a parabolic shape at any point of the fiber). These parabolic pulses are in fact exact asymptotic solutions of the Nonlinear Schrödinger Equation with gain . On the contrary, in our experiment where no distributed amplification is applied, the pulses have a parabolic shape only for a limited range of fiber length which depends on the initial pulse power. Consequently, the input average power was optimized to obtain quasi linear chirp across the pulses and minimum overlapping between consecutive pulses at the NZ-DSF output. Optimum power was found to P_0 = 370 mW. Solid line in Fig. 5a represents the parabolic pulse train at the NZ-DSF output. Figures 5c and 5d are the corresponding spectrum and phase

profile, respectively. Clearly, the spectral broadening is associated with the generation of a strong linear chirp across the pulses. A linear dispersive fiber with opposite dispersion (anomalous dispersion) was then used to compress the parabolic pulses. As shown in Fig. 5b, large compression ratio is obtained and the pulse shape corresponds to a nearly Gaussian profile at the center with a FWHM equal to 5.5 ps. Moreover, as the propagation is almost linear, the output spectrum (Fig. 5f) is identical to the input spectrum (Fig. 5c). On the other hand, we can see that the pulses are accompanied by a weak pedestal component. Finally, phase profile of the output pulse train is shown in Fig. 5e and found to be roughly flat in the center part of the pulse only.

3.3 Experimental results

The experimental results obtained at $\lambda = 1550$ nm are shown in Fig. 6. Maximum compression ratio was obtained for an average input power of $P_0 = 400$ mW, in close agreement with the predicted theoretical value. The measured FROG trace (128×128 grid) is plot in Fig. 6c while the retrieved trace is shown in Fig. 6d. The FROG retrieval error was as low as 5.10^{-3}. Solid line in Fig. 6a is the retrieved intensity profile compared with the numerical predictions (circles). We can clearly observed a good agreement between experimental results and numerical simulations, stressing the reliability of the model. Retrieved phase is shown in Fig. 6b and is quite flat around the pulse center. As predicted from numerical simulations, a π phase shift is observed between adjacent pulses.

Finally, for a central wavelength λ varying between 1545 nm and 1565 nm and a constant power of $P_0 = 400$ mW, we have studied the variation of the output pulse profiles. Autocorrelation traces and corresponding spectra, represented in Fig. 7, are found to be very similar for three values of λ between 1545 nm and 1565 nm, demonstrating the tunability of the compression technique over a 20 nm bandwidth.

4 Discussion and conclusion

The different results presented in sections 2 and 3 lead to important conclusions about the two methods. Pulses generated from the compression of parabolic pulses can be very narrow but are, in general, accompanied by a pedestal component. On the other hand, the multiple FWM compression technique permits to obtain high-quality transform-limited Gaussian pulses. However, this method is based on the presence of localized bands in the intensity spectrum and thus requires a stricly periodic pulse train. As a consequence,

compression is strongly affected by the presence of "zero" marks in a bit sequence. This behaviour is illustrated in Fig. 8b where we have numerically calculated the temporal compression of a coded input sinusoidal signal. Clearly, the shape of a given pulse depends on its position in the bit sequence, which is a strong limitation of this method. The second method, based on the nonlinear transformation of each individual pulse into a parabolic pulse, does not suffer of this drawback. Figure 8c illustrates the superiority of the parabolic method for coded pulse trains. Fig. 9 represents the compressed pulses obtained from numerical simulations when no phase shift is present between adjacent pulses. From Fig. 8 and Fig. 9, we clearly see that the output pulses profiles obtained through the multiple FWM compression technique are very sensitive to both the phase and the bit patterns of the incident pulse train, which is not the case with the second method based on parabolic pulses generation. Finally, note that the compression factor obtained from the two techniques are about 2.3 and 4.5 respectively. Clearly, higher compression factors can be obtained using adiabatic soliton compression methods (see for example Ref. where a compression factor of 17 is obtained). However, such methods are often difficult to achieve since they require a careful management of the dispersion profile of the fibers. Nevertheless, by considering that in RZ telecommunication systems, the pulse width is typically between 33 % and 50 % of the bit slot, we found that the 11 ps-pulses obtained by the multiple FWM compression technique are suitable for generating 40 Gb/s telecommunication pulse trains whereas the 5.5 ps-pulses, generated from the parabolic pulse compression, could be multiplexed to obtain pulse trains at bit rates as high as 80 Gb/s.

5 Acknowledgements

The authors acknowledge financial support of this research by the Conseil Regional de Bourgogne, the Centre National de la Recherche Scientifique and the Ministère de la Recherche et des nouvelles Technologies.

References

A. Hasegawa, Opt. Lett. **9**, 288 (1984).

K. Tai, A. Tomita, J.L. Jewell and A. Hasegawa, Appl. Phys. Lett. **49**, 236 (1986).

P.V. Mamyshev, S.V. Chernikov and E.M. Dianov, IEEE J. Quantum Electron. **27**, 2347 (1991).

S.V. Chernikov, J.R. Taylor, P.V. Mamyshev and E.M. Dianov, Electron. Lett. **28**, 932 (1992).

S. Pitois, J. Fatome and G. Millot, Opt. Lett. **27**, 1729 (2002).

R. Trebino, K.W. Delong, D.N. Fittinghoff, J.N. Sweetser, M.A. Krumbugel, B.A. Richman and D.J. Kane, Rev. Sci. Instrum. **68**, 3277 (1997).

F. Gutty, S. Pitois, P. Grelu, G. Millot, M.D. Thomson and J.M. Dudley, Opt. Lett. **24**, 1389 (1999).

C. Billet, J.M. Dudley, N. Joly and J.C. Knight , Opt. Exp. **13**, 3236 (2005).

J.A.R. Williams, I. Bennion and L. Zhang, IEEE Phot. Tech. Lett. **7**, 491 (1995).

G. Lenz, B.J. Eggleton and N. Litchnitser, J. Opt. Soc. Am. **15**, 715 (1998).

G.P. Agrawal, Nonlinear Fiber Optics, 3rd ed. (Academic Press, New York, 2001).

M.E. Fermann, V.I. Kruglov, B.C. Thomsen, J.M. Dudley and J.D. Harvey, Phys. Rev. Lett. 84, 6010 (2000).

K. Igarashi, H. Tobioka, M. Takahashi, T. Yagi and S. Namiki, Electronics Letters 41, 797 (2005).

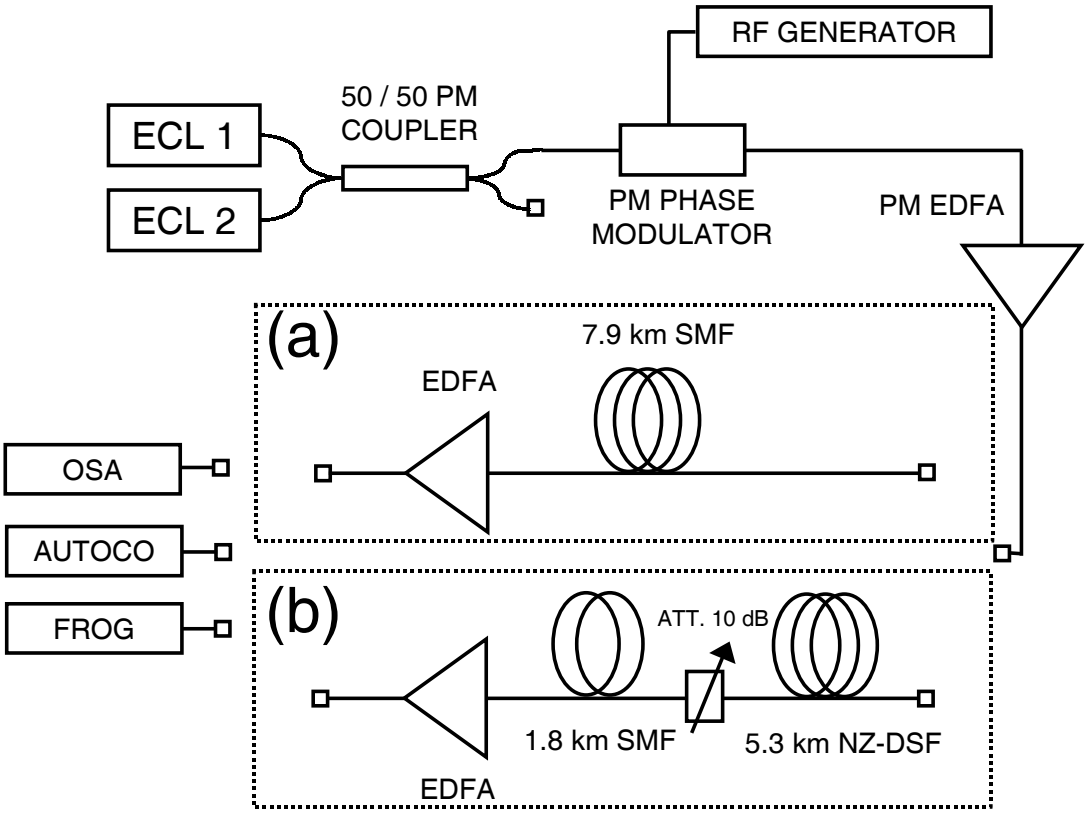

Fig. 1. Experimental setup. ECL : external-cavity laser, PM : polarization-maintaining, EDFA : erbium-doped fiber amplifier, ATT : attenuator, OSA : optical spectrum analyser, AUTOCO : background-free second-harmonic-generation autocorrelator, FROG : Frequency Resolved Optical Gating. (a) configuration used for multiple FWM compression, (b) configuration used for parabolic pulses generation and linear compression.

Figure 1, S. Pitois et al.

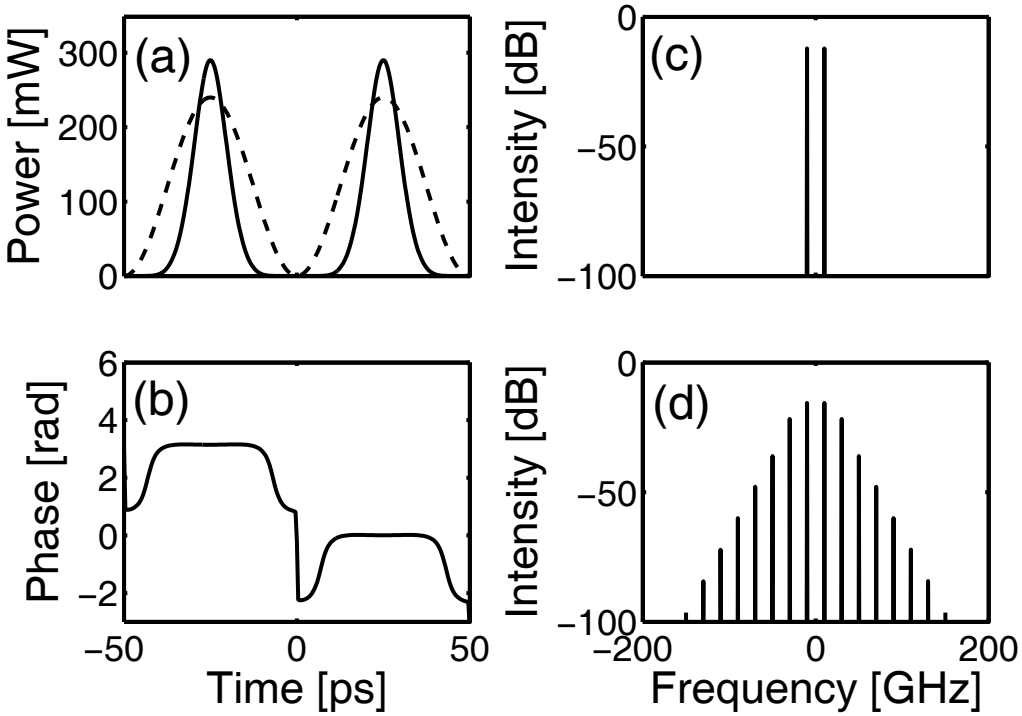

Fig. 2. Numerical simulations results of transformation of a beat signal into a train of short pulses using FWM technique and for an input average power of 120 mW. (a) Intensity of the compressed pulse train (solid curve) and the input beat signal (dashed curve). (b) Phase variation of the compressed pulses. (c) Spectrum of the input signal. (d) Spectrum of the compressed pulse train.

Figure 2, S. Pitois et al.

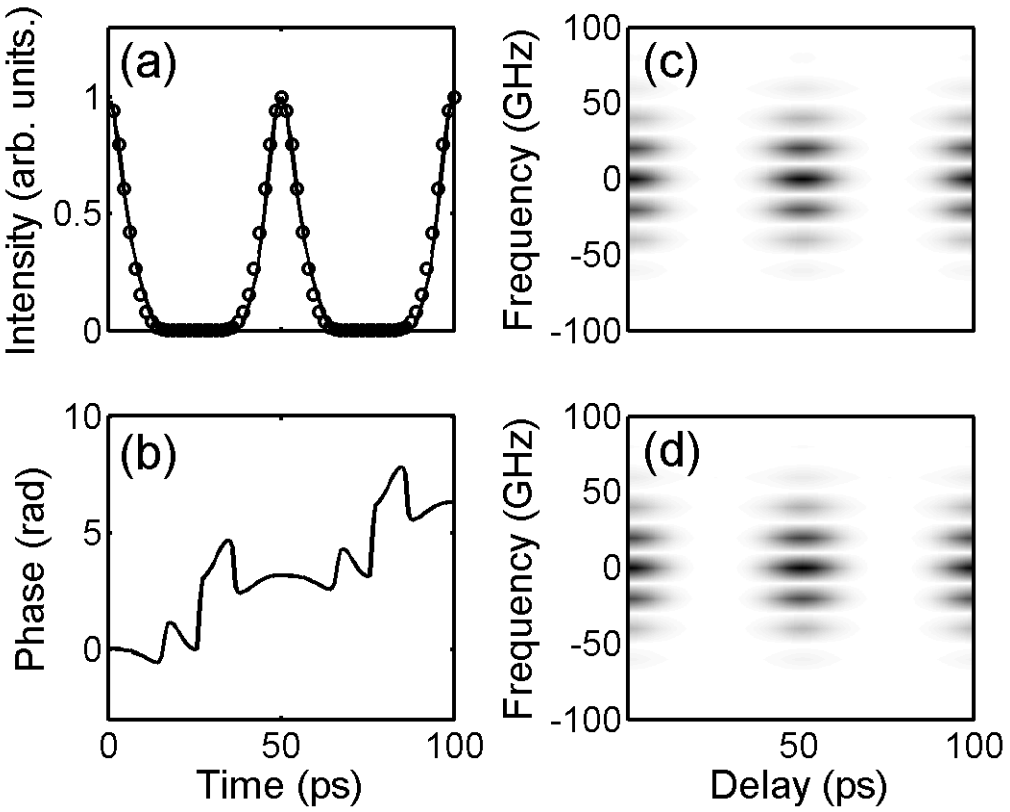

Fig. 3. Experimental results : (c) Measured and (d) retrieved SHG-FROG traces of the 20 GHz generated pulse train. (a) solid curve : retrieved intensity , circles : numerical simulations. (b) Retrieved phase.

Figure 3, S. Pitois et al.

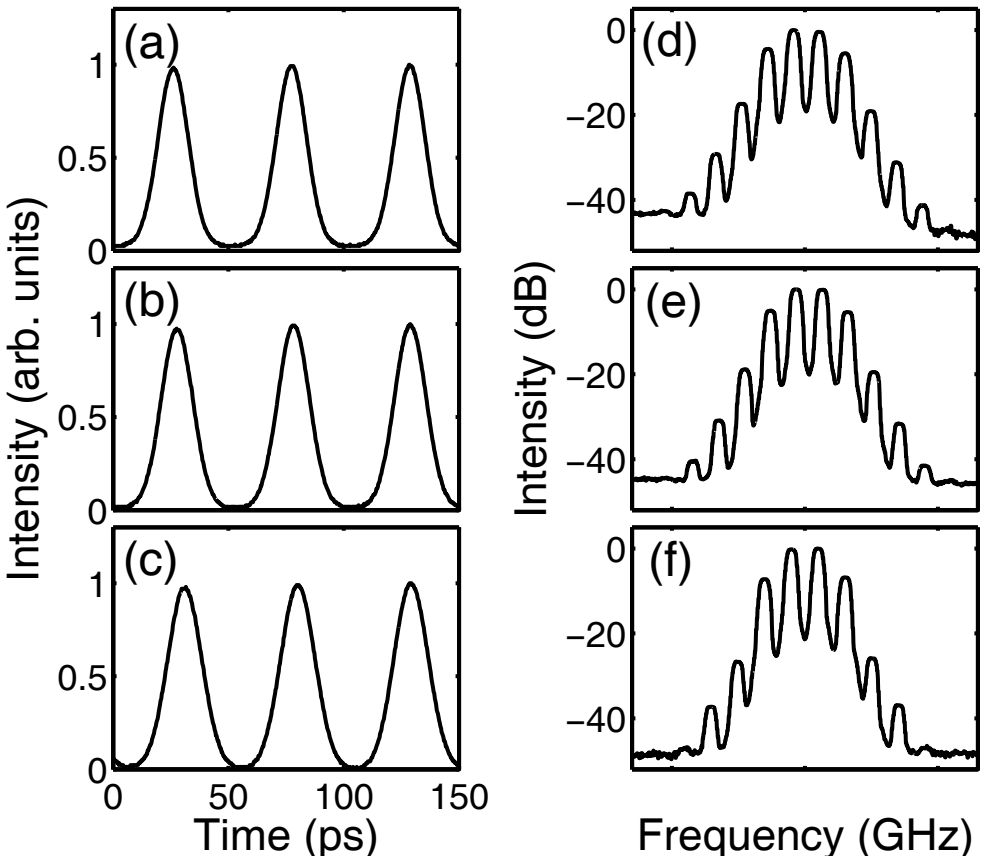

Fig. 4. Measured autocorrelations (left column) and spectra (right column) of the compressed pulse train obtained by the FWM technique for (a), (d) : $\lambda = 1545$ nm, (b), (e) : $\lambda = 1550$ nm and (c), (f) : $\lambda = 1565$ nm.

Figure 4, S. Pitois et al.

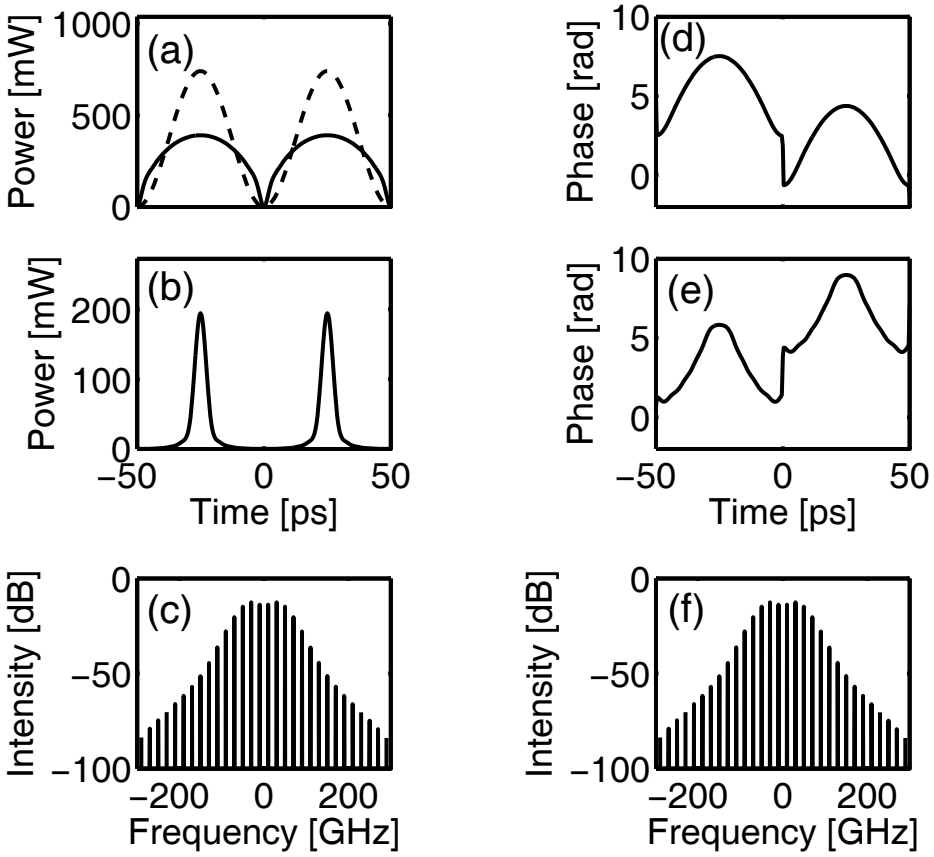

Fig. 5. Numerical simulations results of transformation of a beat signal into a train of short pulses using parabolic pulse technique and for an input average power of 370 mW. (a) Intensity of the parabolic pulse train at the NZ-DSF output (solid curve) and the input beat signal (dashed curve). (d) Phase variation of the parabolic pulses. (b) Intensity profile of the compressed pule train at the SMF output. (e) Phase variation of the compressed pulses. (c),(f) : Spectra of the pulse train at the NZ-DSF output and SMF output, respectively.

Figure 5, S. Pitois et al.

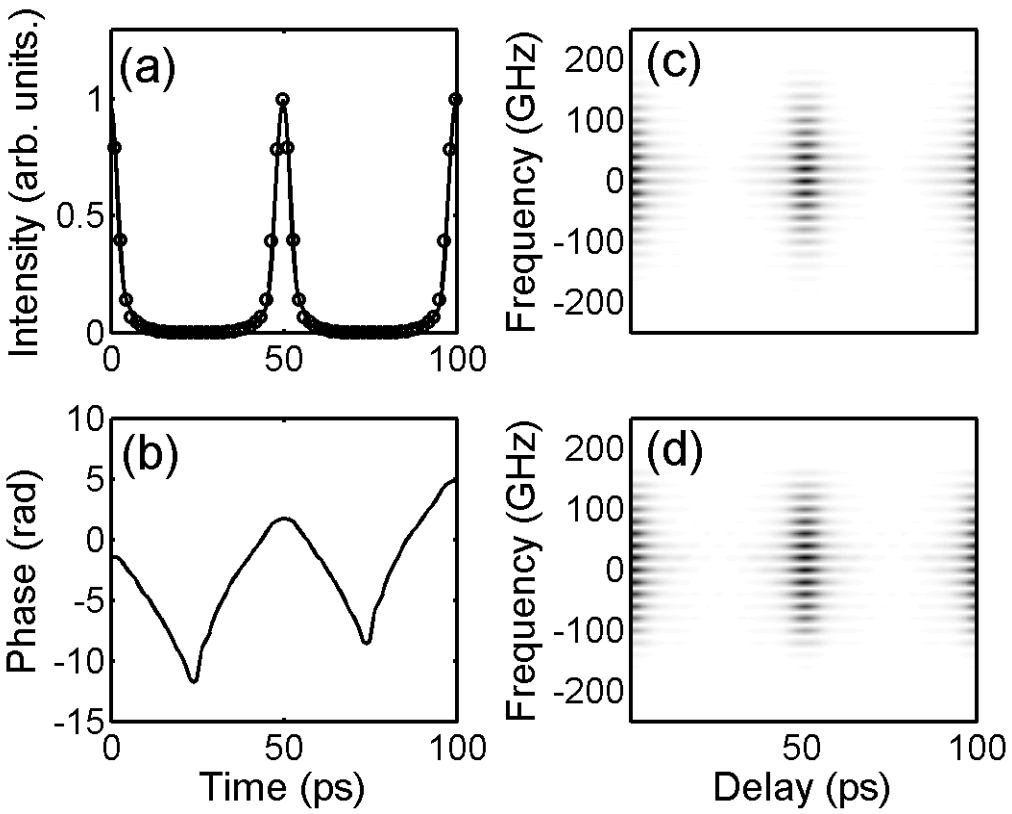

Fig. 6. Experimental results : (c) Measured and (d) retrieved SHG-FROG traces of the 20 GHz generated pulse train. (a) solid curve : retrieved intensity , circles : numerical simulations. (b) Retrieved phase.

Figure 6, S. Pitois et al.

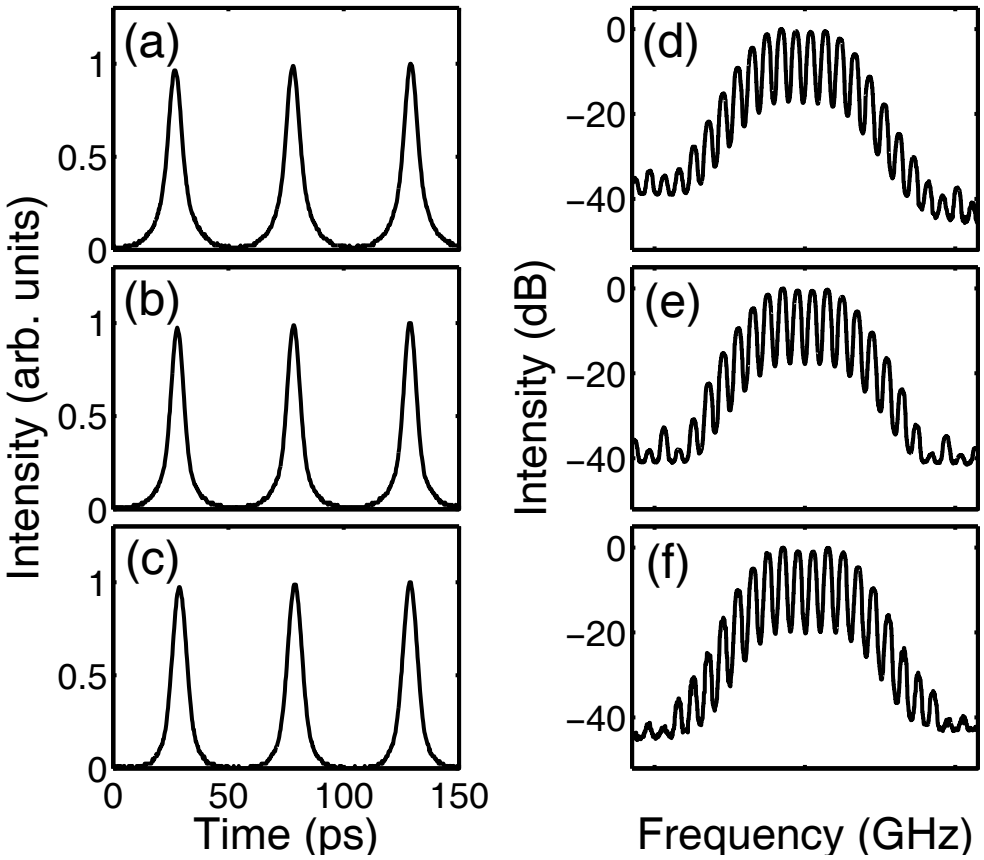

Fig. 7. Measured autocorrelations (left column) and spectra (right column) of the compressed pulse train obtained by the parabolic pulse generation technique for (a), (d) : $\lambda = 1545$ nm, (b), (e) : $\lambda = 1550$ nm and (c), (f) : $\lambda = 1565$ nm.

Figure 7, S. Pitois et al.

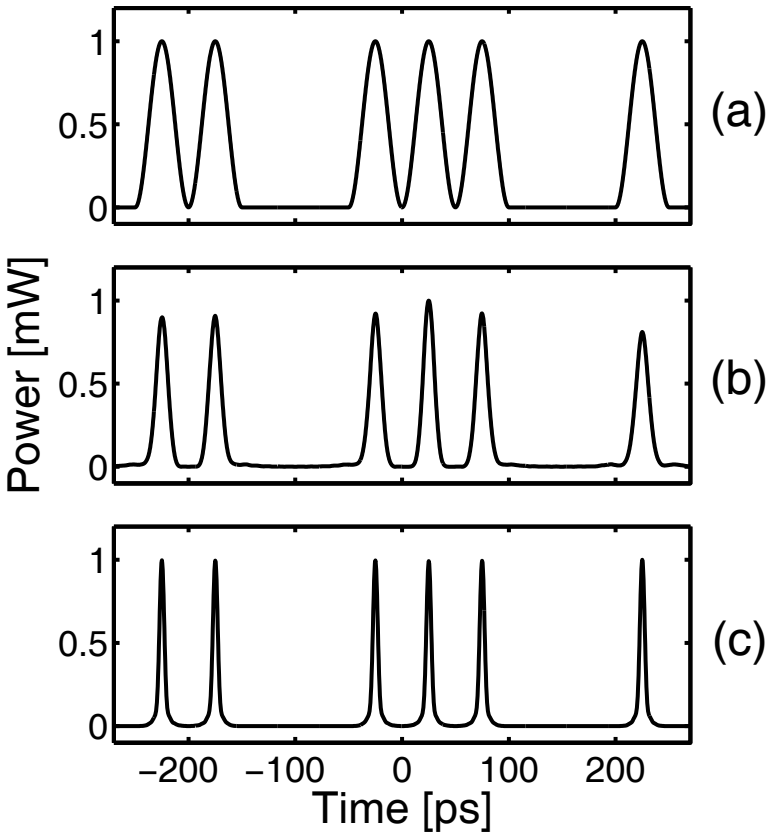

Fig. 8. Results of numerical simulations of compression of a coded beat-signal with a π phase shift between consecutive pulses. (a) input coded beat signal, (b) compressed pulse train using the multiple FWM technique, (c) compressed pulse train by using parabolic pulse generation technique.

Figure 8, S. Pitois et al.

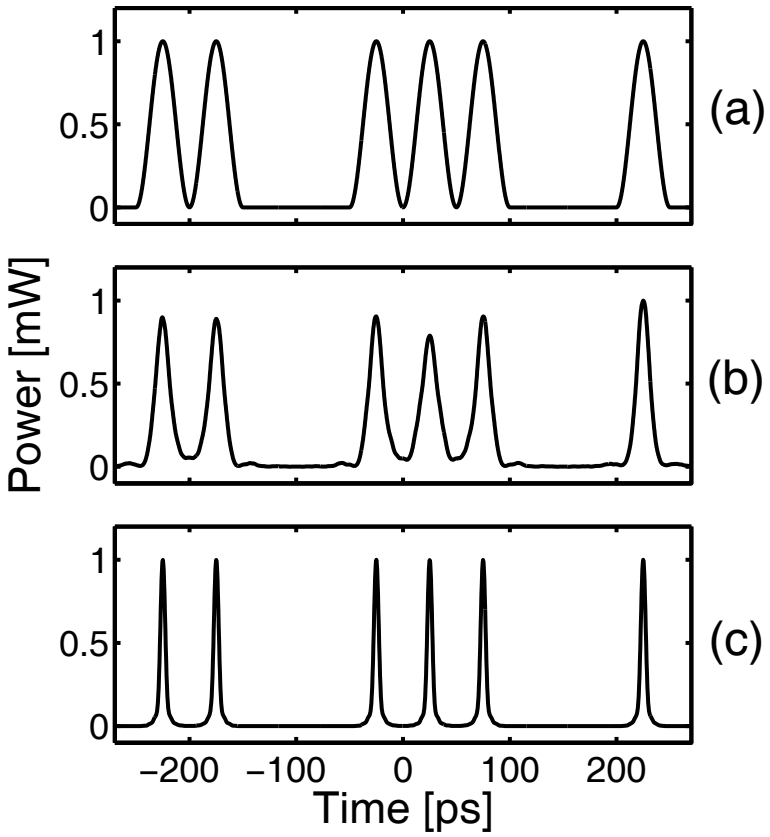

Fig. 9. Results of numerical simulations of compression of a coded-beat signal without any phase shift between consecutive pulses. (a) input coded beat signal, (b) compressed pulse train using the multiple FWM technique, (c) compressed pulse train by using parabolic pulse generation technique.

Figure 9, S. Pitois et al.